ADVANCED OPTICAL MATERIALS
www.advopticalmat.de

Soft Photonic Fibers for Colorimetric Solvent Vapor Sensing

Mirela Malekovic, Markus Urann, Ullrich Steiner, Bodo D. Wilts, and Mathias Kolle**

Stimuli-responsive elastomers are promising material systems for the development of optical sensors with visual outputs that can be easily assessed by the human eye. These materials, when shaped into alternating layers, form distributed Bragg reflectors (DBRs) that feature a high spectrally selective reflectivity. The adsorption of vapor molecules into these photonic structures leads to partial swelling in the constituent materials that can induce pronounced color changes. Here, it is demonstrated that soft photonic fibers with a DBR-cladding can selectively sense and quantify different organic vapors. It is found that fibers with a multilayer cladding assembled of films of polydimethylsiloxane (PDMS) and a polystyrene-polyisoprene block-copolymer (PSPI) change color sensitively depending on the concentration of toluene, benzene, tetrahydrofuran, or chloroform vapors. It is shown that this is a direct consequence of a selective swelling of the constituent polymer layers due to vapor adsorption. With wavelength variations as small as 5 nm being noticeable to the human eye, such photonic fibers are interesting materials for optical sensors. Modifications of their building blocks and their structural morphology make these vapor-sensing fibers a versatile platform for standalone and textile-integrated solvent sensing systems applied in industrial and lab-scale manufacturing processes.

1. Introduction

Coherent scattering from a periodic multilayer structure, a so-called distributed Bragg reflector (DBR), results in highly reflective, iridescent structural color. DBR structures for light manipulation are employed by many organisms in nature[1–7] and have found use in various devices and industrial applications.[8–13] Colors resulting from the interference of light in periodic arrays have numerous advantages over chemically-derived pigmentary colors, such as long-term stability.[14,15] Photonic structures composed of reconfigurable, stimuli-responsive, inexpensive and commercially available materials,[16,17] including elastomeric polymers,[18,19] hydrogels,[20–22] or colloids,[23–25] have gained increasing interest over the last years. These colored materials can alter their configuration, shape, mechanical behaviour, and optical characteristics in response to a variety of stimuli[18,22,24,26,27] and are therefore versatile platforms for the design of stimuli-responsive sensors.

Soft photonic fibers rely on the interference of light reflected from periodically arranged optical interfaces in 100-nm-scale architectures, which are assembled from soft materials with different refractive indices. Such fibers can be designed to reflect light in only a selected part of the visible spectrum, or a broadband manner. Their fabrication can be achieved in several ways, including thermal drawing, extrusion, and self-assembly.[13,28,29] Besides, the rolling of thin elastomer film bilayers around an elastic core allows creating fibers with a mechano-responsive Bragg reflector cladding at room temperature.[30] The microscale curvature of the multilayer cladding gives rise to wavelength-selective light scattering into a wide range of directions, while its spectral reflection band is comparable to that of a flat Bragg stack with similar layer thicknesses. This established rolling technique allows the facile assembly of Bragg reflectors with a high number of layers to form fibers with a reflectivity that can exceed 90%. The spectral location and intensity of their reflection band critically depend on the refractive index difference of the employed materials and the layer thicknesses, which can easily be tuned by controlling the process parameters during fiber formation.

Solvent-permeable Bragg reflectors are in principle suited to sense environmental vapors. Reversible adsorption and desorption of solvent vapors within the structure causes an effective refractive contrast, resulting in a change in coloration. The optical response of such solvent-permeable photonic systems to vapor sorption depends on features, such as the presence and size of pores, surface textures, and nature of the constituent materials, combined with the interaction between neighboring layers.[31] The chemical properties of the cladding material[32,33] in combination with the vapor type[34] and concentration[35] determine whether capillary condensation of vapor molecules occurs within the structure, which can lead to a variety of effects. For instance, the refractive index of porous inorganic

M. Malekovic, Prof. U. Steiner, Dr. B. D. Wilts
Adolphe Merkle Institute
University of Fribourg
Fribourg CH-1700, Switzerland
E-mail: bodo.wilts@unifr.ch
M. Urann, Prof. M. Kolle
Department of Mechanical Engineering
Massachusetts Institute of Technology
Cambridge, MA 02139, USA
E-mail: mkolle@mit.edu
The ORCID identification number(s) for the author(s) of this article can be found under https://doi.org/10.1002/adom.202000165.

DOI: 10.1002/adom.202000165

materials changes when the air in the pores is replaced with a higher refractive index compound.[32] For organic materials, vapor absorption can result in multiple phenomena, ranging from swelling of the layers to variations in effective refractive index.[33] The cumulative effect of these vapor-induced phenomena in inorganic and organic structured materials is a noticeable shift of the reflection band to longer wavelengths.

Here we demonstrate that polymeric soft photonic fibers can be employed to detect organic solvent vapors quantitatively. Vapor-induced color variations are a useful visual indicator that can be used in a versatile platform for cheap and easily manufactured optical organic vapor sensors. The changes in fiber colour can be perceived by the human eye, which provides an opportunity for sensor designs that rely on visual assessment without the need for sophisticated spectral detection equipment.

2. Results

A previously established rolling technique was employed to produce highly reflective multilayered photonic fibers[18] (see the Experimental Section). A double layer of two different elastomers was floated onto a water surface and then rolled around a cross-linked polydimethylsiloxane (PDMS) fiber. The employed elastomers for double layer manufacture were PDMS and a polyisoprene-polystyrene (PSPI) block copolymer. These two materials have comparable mechanical properties, can be spin-coated into thin films, have different refractive index values (1.41 ± 0.02 for PDMS and 1.54 ± 0.02 for PSPI, determined by ellipsometry), and are commercially available and affordable. PDMS is an optically transparent, widely-used elastomer that can be chemically cross-linked at temperatures of 60–150 °C. PSPI triblock terpolymers are thermoplastic elastomers consisting of polyisoprene (PI) chains with covalently linked polystyrene (PS) blocks on both chains ends. Microphase separation of the PSPI block-copolymer results in physically cross-linked glassy PS domains inside an elastomeric PI matrix without additional curing steps. In our experiments, the individual thickness of the PDMS and PSPI were optimized to maximise reflectivity of the rolled fibers in the green part of the visible spectrum, resulting in layer thicknesses of 91 ± 3 and 100 ± 3 nm, respectively, as measured by ellipsometry. Other colors can be achieved by adjusting the film thicknesses.[11] The final thickness of the multilayered cladding rolled on a 470 µm diameter elastic core fiber was determined by scanning electron microscopy (SEM). Roughly 70 alternating PDMS/PSPI layers correspond to cladding thickness of 7 µm (**Figure 1**b).

When exposed to vapors of "good" solvents, polymer films change their thickness by swelling. A polymeric DBR is, therefore, an excellent vapor sensor, since the swelling of individual layers through solvent absorption results in visible color changes. A schematic of the sensing mechanism is shown in Figure 1a. Here, we assess the optical response of DBR fibers exposed to vapors of toluene, heptane, benzene, THF, chloroform and acetone, organic solvents often used in industrial and academic laboratories. All experiments were performed at room temperature and atmospheric pressure (T = 293 K, p = 101.3 kPa). The different solvents have different vapor pressures, and hence their saturation concentration in air varies. In the experiments, the mixing ratio between dry nitrogen and nitrogen saturated with solvent vapor was controlled.

Exposing the soft fibers to a vapor of toluene results in a significant spectral shift (**Figure 2**). The reflection of an initially green fiber undergoes a gradual change towards longer wavelengths with increasing vapor concentrations (Figure 2a). For example, for each 1% of toluene vapor, the reflectance spectrum of the fiber shifts by about 41 nm (Figure 2b). The absorption of 3% of toluene induced a shift of the reflectance band to the near-infrared, and the color was lost to the human eye (lower right image of Figure 2a).

Next, we tested the response of the fibers to a range of different solvents. Benzene, THF and chloroform solvent vapors resulted in pronounced spectral shifts with different sensitivities for each solvent (**Figure 3**a), although all responses were less sensitive than the response to toluene. Absorption of 1% of benzene caused a spectral shift of ≈7 nm while the same amount of THF and chloroform resulted in a spectral shift of ≈3 nm (Table T1, Supporting Information). For these solvents, the spectral change was much smaller than for toluene, and a shift to the near-IR part of the spectrum was not observed, even though the highest tested concentrations were several times higher than the highest toluene concentration. Figure 3b shows that exposure of the fiber to heptane and acetone resulted in negligible variation of fiber color, indicating that the multilayer cladding did not swell in the presence of these organic vapors.

The fibers' color response when exposed to chloroform could be reversibly cycled when alternating between dry and a solvent-rich atmosphere (**Figure 4**). The color change is fast (within seconds) for small variations in solvent vapor concentration. However, drying of a saturated fiber is slower, and a full vapor removal resulting in a shift from red to green takes about 10 min.

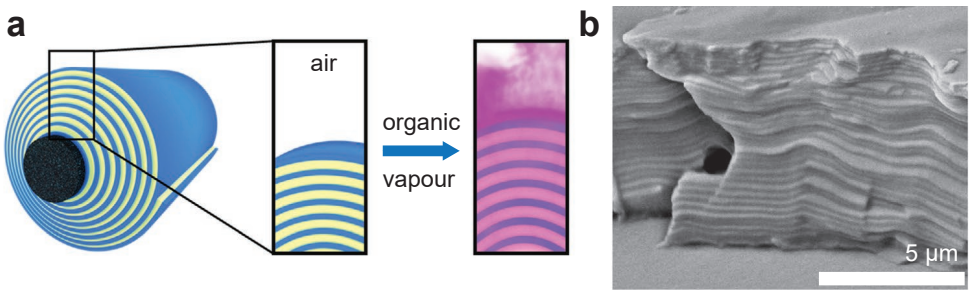

Figure 1. a) Schematic cross-section of photonic fiber and color change sensing mechanism based on the adsorption of an organic solvent into polymer material followed by swelling. b) SEM image of the cross-section of the rolled PDMS/PSPI multilayered cladding.

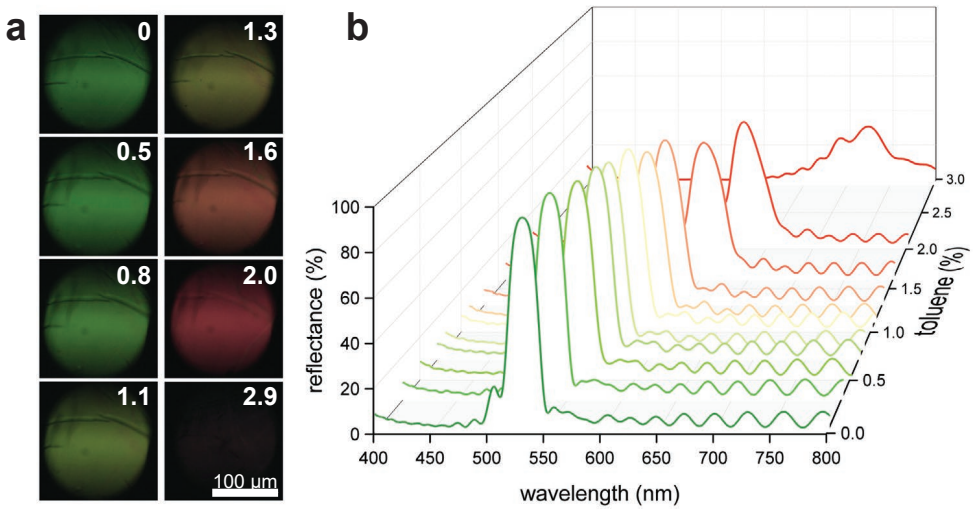

Figure 2. a) Micrographs of a fiber's surface, showing the color change when exposed to different concentrations of toluene vapor (%). The top left image is of fiber in air and bottom right of fiber in high toluene concentration. b) Change of the reflectance spectra for the representative fiber. Absorption of 3% of toluene induced a shift of the reflectance band to the near-infrared, and the color was lost to the human eye (bottom right image in (a)).

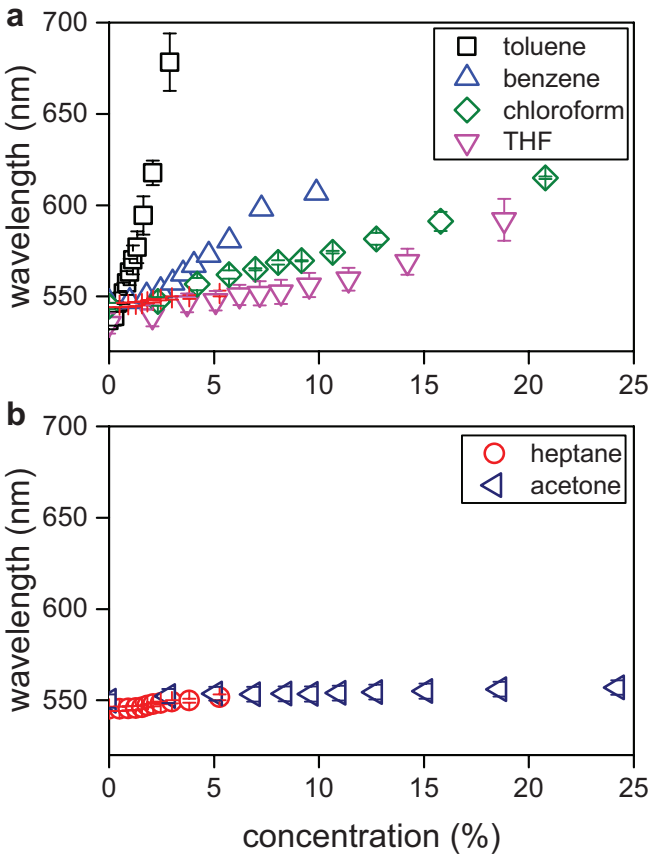

Figure 3. Change of peak reflectance for fibers exposed to different concentrations of a) toluene, benzene, THF, and chloroform, and b) heptane and acetone. Toluene results are averaged over measurements from eight fibers, and results for heptane, benzene, THF, chloroform, and acetone are averages over measurements on three different fibers. The error bars represent standard error of the mean.

To assess the degree of swelling in the fibers' polymer layers, the thickness changes of thin homopolymer films of either PDMS or PSPI upon exposure to organic vapors were measured. **Figure 5** shows the swelling ratio for these films as determined by optical spectroscopy. Thin films of both polymers significantly swell in the various organic vapors. PSPI films swell slightly more in most vapors than the cured PDMS films, and the response of the homopolymer films corresponds in strength to that of the multilayer fibers: the response to toluene was the strongest, followed by benzene, THF and chloroform. The weakest response was measured for acetone, but surprisingly both PSPI and PDMS single film swell strongly when exposed to heptane vapors, in contrast to the absence of apparent swelling in the multilayer fibers.

The core fiber fabricated from a mixture of PDMS and black silicon dye was also exposed to organic solvents. Here, the observed swelling ratio in heptane and THF was the highest, followed by toluene, chloroform and benzene, while it was low for acetone (Figure S3, Supporting Information).

The differences between the swelling behaviour of individual thin films and the multilayer fiber cladding are due to different mechanical constraints acting on the supported single films of Figure 5, and the rolled-up DBRs presented in Figures 1–4. In supported single films, swelling causes an elongational stress perpendicular to the film surfaces and, though the inhibition of Poisson contraction, a weak in-plane biaxial tensile stress. The combination of these two stresses limits film expansion at a given vapor pressure of good solvents. In the DBR fibers, however, the stress distribution differs. The swelling of the core and the lower-lying DBR layers result in a radius increase for a given layer position. This leads to a substantial circumferential tensile stress in that layer, an effect which increases with increasing radial position of the layer. This tensile stress is much larger than the Poisson-induced tensile stress of the corresponding planar

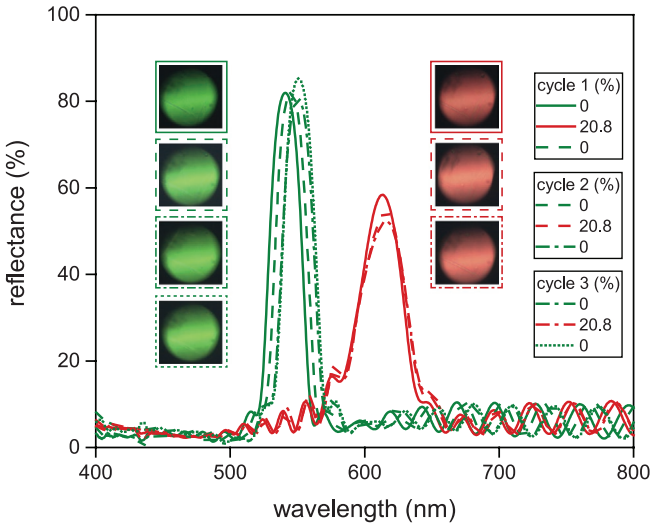

Figure 4. Color change of a fiber placed in an organic vapor is reversible. The fiber is green when placed in a pure nitrogen atmosphere and changes color to red with a chloroform concentration of ≈20.8%. When chloroform vapor is removed, the color changes back to green within a few minutes. Adding and removing of chloroform was performed in three consequent cycles, optical micrographs showing change of color of a single spot of the same fiber.

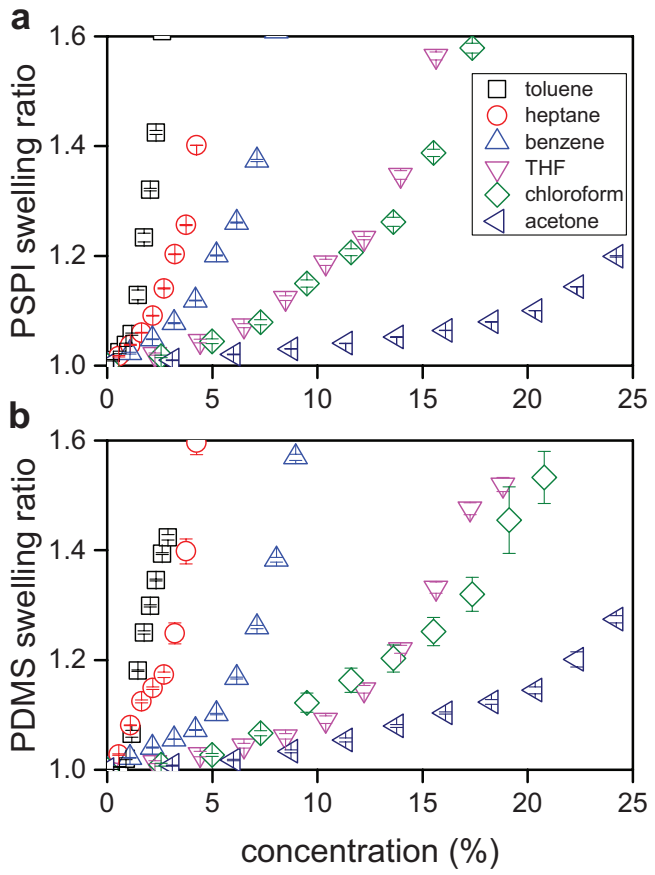

Figure 5. Swelling ratio versus concentration change for homopolymer thin films: a) PSPI and b) PDMS. All the measurements are averaged over three times. Error bars represent standard error of the mean.

films, thereby restricting swelling to a much larger degree. This qualitative argument is borne out by the comparison of the individual polymer films, which swell up to ≈80% in a saturated atmosphere, with the fibers that maximally increase in (effective) thickness by ≈20–30%, as deducted from the wavelength change upon swelling (Figure 3). In other words, the radial DBR layers swell less by a factor of 3–4 compared to the planar reference films (see also **Table 1**).

This explains the lack of swelling of the multilayer fibers exposed to acetone and heptane (Figure 3). Both PSPI and PDMS single films swell only weakly when exposed to acetone, so that the added tensile stress imposed by the swelling of the core completely supresses film thickness variations in the multilayer fibers. In contrast, PSPI and PDMS single films swell very strongly in heptane, making the lack of color variation of multilayer fibers exposed to vapor of this solvent surprising. The explanation for this discrepancy is the strong swelling of the core fiber (Figure S3, Supporting Information), so that the induced tensile stress in the multilayer cladding overpowers single layer swelling. This effect is also visible for THF, where a moderate single-layers swelling response gives rise to only a weak color variation as the THF vapor concentration is increased.

In this context, since layers at the varying radial positions are differently stretched, their effective thickness increase varies, which causes the detuning of the optical band-gap. This is borne out by the spectra in Figure 2 and Figure S2 (Supporting Information), where both the reflected peak intensity reduces, and the spectral shape broadens with increasing swelling ratio. The quantitative description of the interplay of stretching, swelling and the ensuing optical response is, while possible,[11,18,30] not straight forward, since all physical parameters (elastic modulus, refractive index) are a function of solvent concentration within the polymer, leading to a complex interplay of the discussed mechanical and optical mechanisms.

3. Discussion

The photonic fibers presented here are a versatile colorimetric sensor for measuring the vapor concentrations of various solvents, with a sensitivity of around 1000 ppm (0.1%). The color change arises from the swelling of the components of the Bragg stack. When exposed to low concentrations of these solvents, the fibers change color due to the simultaneous swelling of the PSPI and PDMS films in the multilayer cladding (Figure 3). The fibers are particularly susceptible to toluene vapor with a spectral shift of 1 nm per ≈250 ppm (0.025%) of the absorbed solvent. The solvent-induced color change is reversible and can occur multiple times without degradation of the fiber or obvious change in the optical response (Figure 4).

By varying the constituent materials of the soft photonic fiber, the proof-of-concept fiber-based system presented here could be made sensitive (exclusively) to specific vapors of interest.[36] This could, for example, be achieved by selective functionalization of one or both building blocks, or altering the core of the fiber. For example, Torino et al. used functionalized PDMS membranes as sensing elements in optical sensors for detection of methanol in water,[37] while other polymers, like poly(methyl methacrylate) or poly(vinyl pyrrolidone), can be

Table 1. Slope values of swelling ratios (SRs) per 1% of the solvent for homopolymer thin films (PDMS and PSPI), calculated swelling ratio of core fiber, the spectral shift of the fibers reflectance per 1% of the solvent, and vapor sensitivity of the fibers per ppm of the solvent. Linear regression was used to fit the experimental data within lower vapor concentration ranges.

Solvent	PDMS thin film slope [SR per 1%]	PSPI thin film slope [SR per 1%]	Core fiber calculated swelling ratio	Fiber spectral sensitivity [nm per 1%]	Fiber vapor sensitivity [ppm per 1 nm]	Refractive index (D-line[52–56])
Toluene	0.163 ± 0.011	0.197 ± 0.025	1.43	41.16 ± 3.24	250	1.4920
Benzene	0.071 ± 0.013	0.136 ± 0.031	1.41	6.96 ± 0.44	1450	1.4956
Chloroform	0.025 ± 0.003	0.042 ± 0.006	1.43	3.30 ± 0.14	3050	1.4440
THF	0.027 ± 0.004	0.052 ± 0.009	1.48	2.75 ± 0.21	3650	1.4050
Heptane	0.204 ± 0.037	0.188 ± 0.044	1.51	1.37 ± 0.10	7250	1.3888
Acetone	0.01 ± 0.001	0.0069 ± 0.001	1.07	0.26 ± 0.03	38750	1.3591

functionalized for specific use as pH or humidity sensors.[38,39] Similar structural colors systems already proved to be useful sensors for organic solvent mixtures.[34,40] Another possible approach to disentangle and more precisely determine gas combinations might be possible through combinatorial sensing with multiple fibers that are assembled from different polymer combinations, with post-hoc signal analysis using principal component analysis, as recently performed by Mao et al.[41]

The physical principle of the soft fiber-based photonic vapor detector is different from previously reported vapor-sensitive light guides.[42,43] In these, the vapor is sensed either by infiltration into a fiber or is in direct contact with it. In our system, the sensing results from a physicochemical interaction of the solvent with the material, resulting in a swelling and refractive index change that affects the interference of incident light within the Bragg reflector cladding of the fiber. We demonstrate vapor sensing via the fibers' easily perceived color variation in vapors of different organic solvents (Figures 3 and 4), after having established the swelling response of individual PDMS and PSPI layers in these vapors.

Both polymers, PDMS and PSPI, swell in vapors of toluene, benzene, THF, and chloroform (Figure 5). However, the extent of the response differs from solvent to solvent. This is comparable to other organic/inorganic sensors or different architectures where physical stimuli govern the color change.[11,18,27,44,45] The color change is also comparable to sensors for solvent/vapor sensing working on the same swelling principle, such as PS nanoparticles incorporated into PDMS matrix, which swell when placed into a non-polar solvent,[40] or the swelling of composite colloidal crystal films.[26] The swelling response could be further improved by employing core fibers that swell only very little in the solvents of interest, such as solvent incompatible polymer fibers, carbon fibers, or inorganic fibers. Depending on the desired application, the interplay of solvent affinity and fiber elasticity/brittleness may however need to be considered.

We envision the use of the vapor-sensing photonic fibers in environments with high organic vapor concentration where conventional electricity operated sensors represent a potential explosion hazard.[46] Because of the polymeric building materials, these sensors are not susceptible to electrical and magnetic fields or water vapor. Furthermore, if soft photonic fibers are used as standalone sensing materials, the color change induced by a small concentration of vapor uptake is noticeable to the human eye, which for instance is the case for toluene vapors. The responsive photonic multilayer structures in fiber form provide opportunities for their integration in woven structures[11] that provide sensing elements in textiles and next-generation wearables.[47]

The function of the sensors as warning signs for humans critically depends on the sensitivity of the fiber to vapor concentrations of a specific solvent and the sensitivity of the human eye to changes in fiber hue.[48] Human color vision relies on three types of cone cells with peak sensitivity at ≈445, ≈535, and ≈575 nm respectively.[49] As a consequence of the spectral composition, the human visual system is most sensitive to wavelength changes in the green part of the spectrum, in a band around 555 nm.[50] In this central part of the spectrum, spectral changes of only 1–2 nm can be detected, while at the extremes of the human-visible range (380–420 and 720–800 nm, respectively), the noticeable difference rises to as much as 20 nm.[51] This suggests that photonic fibers should be green, rather than blue or red, to detect small vapor concentrations with the human eye. When combined with a spectrometer, green and blue soft photonic fibers have potential as vapor-detecting optical sensors.

4. Experimental Section

Fiber Fabrication: A double layer of polydimethylsiloxane (PDMS, Sylgard 184, Dow Corning) and polystyrene-polyisoprene-polystyrene triblock copolymer (PSPI, Sigma Aldrich, 17 wt% content polystyrene) was the principal component for the manufacture of soft photonic fibers. To form this bilayer, a water-soluble sacrificial layer of polystyrene-sulfonic acid (PSS, Sigma Aldrich, 3 wt% solution in water) was first spin-coated onto a pre-cleaned silicon wafer. Subsequently, a thin film of polydimethylsiloxane (3 wt% in heptane) was deposited on top of the sacrificial PSS layer. The PDMS layer was subsequently cured at 70 °C in an oven for 2 h. A thin film of a polystyrene-polyisoprene-polystyrene triblock copolymer (2 wt% in toluene) was then spin-coated on top of the cross-linked PDMS thin film to form a bilayer.

To fabricate the fiber, the double layer coated wafer was slowly immersed into a water bath at an angle of around 35°. As the sacrificial PSS layer dissolves, the bilayer detaches from the silicon wafer and floats on the water surface. An elastomeric core fiber (PDMS, SE 1700, Dow Corning) was manufactured by extrusion of a mixture of PDMS and Silc Pig silicone pigment dye (Smooth-O), followed by curing.[11] The core fiber was then attached to the one edge of the rectangular floating layer by adhesion to the PSPI layer. Rotating the fiber at 10–20 turns per minute forms a multilayer cladding on the fiber. Samples were stored in a dark and dry place after rolling to ensure mechanical and optical stability.

A customised microscope with an integrated solvent vapor sample chamber was employed to investigate the solvent-dependent response

of the soft photonic fibers. Placing fiber samples in this solvent chamber with a transparent quartz window allowed microscopic and spectroscopic optical characterisation of the fibers during exposure to different solvent vapors. A 10 × objective (NA = 0.25) was used to observe the fibers, which were exposed to incident light from a broadband light source (Thorlabs SLS201), coupled into a 200 µm optical fiber and collimated by an aspheric lens before focusing through the objective onto the vapor-sensing fibers. Light reflected from the photonic fibers was collected through the objective and projected by an aspheric lens onto the input window of a 50 µm optical fiber. The other end of this fiber was connected to an Ocean Optics Maya2000 Pro spectrometer (Figure S1, Supporting Information).

The concentration of the solvent vapor was controlled by two streams of nitrogen gas that were introduced into the sample chamber. One stream was saturated with organic solvent vapor by passing through a bubbler. Analogue mass flow controllers (MFC, McMaster-Carr; Variable Area Mechanical Flowmeter, Grainger) were used to control the flow rates of both streams to adjust the relative solvent vapor pressure in the chamber. The saturated solvent vapor pressure (SVP) at ambient conditions was used to calculate the effective concentration of the vapor introduced to the sensing chamber. SVP values (at $T = 293$ K and $p = 101.3$ kPa) of toluene, heptane, benzene, tetrahydrofuran (THF), chloroform, and acetone (Sigma Aldrich) were ≈2.9 kPa, ≈5.3 kPa, ≈10.0 kPa, ≈19.3 kPa, ≈21.1 kPa, and ≈24.6 kPa, respectively. Tested SVP percentages of the organic vapors in nitrogen flow ranged from 0.3%–2.9% for toluene, 0.5%–5.3% for heptane, 1%–9.9% for benzene, 1.9%–17.4% for THF, 2.3%–20.8% for chloroform and 2.8%–24.2% for acetone. Data collection was performed in 1 min intervals. At the beginning of each interval, the solvent concentration was increased by a small increment followed by 1 min wait time for the solvent concentration in the chamber to equilibrate before recording the spectral data.

Supporting Information

Supporting Information is available from the Wiley Online Library or from the author.

Acknowledgements

The authors thank Joseph D. Sandt, Sara Nagelberg, and Cécile A. C. Chazot for support in the lab. This research was financially supported by the National Centre of Competence in Research "*Bio-Inspired Materials*" and the Ambizione program of the Swiss National Science Foundation (168223) to B.D.W.; M.K. and M.U. acknowledge support by the National Science Foundation through the "Designing Materials to Revolutionize and Engineer our Future" program (DMREF-1533985). This project has received funding from the European Research Council (ERC) under the European Union's Horizon 2020 research and innovation programme (grant agreement No. [833895]). M.M., U.S., and B.D.W. acknowledge financial support by the Adolphe Merkle Foundation.

Conflict of Interest

The authors declare no conflict of interest.

Keywords

colorimetric sensors, organic solvent vapors, photonic fibers, polymers

Received: January 29, 2020
Revised: March 23, 2020
Published online: May 4, 2020

[1] F. Schenk, B. D. Wilts, D. G. Stavenga, *Bioinspiration Biomimetics* **2013**, *8*, 045002.
[2] B. D. Wilts, D. G. Stavenga, *Biomimetic Architectures by Plasma Processing: Fabrication and Applications* (Ed: S. Chattopadhyay), Jenny Stanford Publishing, New York **2014**, pp. 1–34, https://doi.org/10.1201/b17862.
[3] P. Vukusic, R. Sambles, C. Lawrence, G. Wakely, *Appl. Opt.* **2001**, *40*, 1116.
[4] S. Kinoshita, S. Yoshioka, *ChemPhysChem* **2005**, *6*, 1442.
[5] S. Yoshioka, T. Nakano, Y. Nozue, S. Kinoshita, *J. R. Soc., Interface* **2008**, *5*, 457.
[6] C. J. Chandler, B. D. Wilts, J. Brodie, S. Vignolini, *Adv. Opt. Mater.* **2017**, *5*, 1600646.
[7] L. Li, S. Kolle, J. C. Weaver, C. Ortiz, J. Aizenberg, M. Kolle, *Nat. Commun.* **2015**, *6*, 6322.
[8] O. Isabella, S. Dobrovolskiy, G. Kroon, M. Zeman, *J. Non-Cryst. Solids* **2012**, *358*, 2295.
[9] V. Shanmugan, M. A. Shah, S. L. Teo, A. Ramam, *Proc. SPIE 5641, MEMS/MOEMS Technologies and Applications II*, December **2004**, https://doi.org/10.1117/12.572816.
[10] K. Iga, K. Kawabata, *Jpn. J. Appl. Phys.* **1975**, *14*, 427.
[11] J. D. Sandt, M. Moudio, J. K. Clark, J. Hardin, C. Argenti, M. Carty, J. A. Lewis, M. Kolle, *Adv. Healthcare Mater.* **2018**, *7*, 1800293.
[12] C. Ryan, C. W. Christenson, B. Valle, A. Saini, J. Lott, J. Johnson, D. Schiraldi, C. Weder, E. Baer, K. D. Singer, J. Shan, *Adv. Mater.* **2012**, *24*, 5222.
[13] B. Gauvreau, N. Guo, K. Schicker, K. Stoeffler, F. Boismenu, A. Ajji, R. Wingfield, C. Dubois, M. Skorobogatiy, *Opt. Express* **2008**, *16*, 15677.
[14] A. R. Parker, D. R. McKenzie, *Proc. R. Soc. B* **2003**, *270*, S151.
[15] S. Kinoshita, S. Yoshioka, J. Miyazaki, *Rep. Prog. Phys.* **2008**, *71*, 076401.
[16] G. Isapour, M. Lattuada, *Adv. Mater.* **2018**, *30*, 1707069.
[17] H.-L. Liang, M. M. Bay, R. Vadrucci, C. H. Barty-King, J. Peng, J. J. Baumberg, M. F. L. D. Volder, S. Vignolini, *Nat. Commun.* **2018**, *9*, 4632.
[18] M. Kolle, A. Lethbridge, M. Kreysing, J. J. Baumberg, J. Aizenberg, P. Vukusic, *Adv. Mater.* **2013**, *25*, 2239.
[19] B. Viel, T. Ruhl, G. P. Hellmann, *Chem. Mater.* **2007**, *19*, 5673.
[20] S. A. Asher, V. L. Alexeev, A. V. Goponenko, A. C. Sharma, I. K. Lednev, C. S. Wilcox, D. N. Finegold, *J. Am. Chem. Soc.* **2003**, *125*, 3322.
[21] A. C. Sharma, T. Jana, R. Kesavamoorthy, L. Shi, M. A. Virji, D. N. Finegold, S. A , Asher, *J. Am. Chem. Soc.* **2004**, *126*, 2971.
[22] E. Tian, J. Wang, Y. Zheng, Y. Song, L. Jiang, D. Zhu, *J. Mater. Chem.* **2008**, *18*, 1116.
[23] Y. Y. Diao, X. Y. Liu, G. W. Toh, L. Shi, J. Zi, *Adv. Funct. Mater.* **2013**, *23*, 5373.
[24] K. Lee, S. A. Asher, *J. Am. Chem. Soc.* **2000**, *122*, 9534.
[25] S.-H. Kim, S. Y. Lee, S.-M. Yang, G.-R. Yi, *NPG Asia Mater.* **2011**, *3*, 25.
[26] A. C. Arsenault, V. Kitaev, I. Manners, G. A. Ozin, A. Mihi, H. Míguez, *J. Mater. Chem.* **2005**, *15*, 133.
[27] S. Kubo, Z.-Z. Gu, K. Takahashi, A. Fujishima, H. Segawa, O. Sato, *J. Am. Chem. Soc.* **2004**, *126*, 8314.
[28] C. E. Finlayson, C. Goddard, E. Papachristodoulou, D. R. E. Snoswell, A. Kontogeorgos, P. Spahn, G. P. Hellmann, O. Hess, J. J. Baumberg, *Opt. Express* **2011**, *19*, 3144.
[29] J. Zhang, S. He, L. Liu, G. Guan, X. Lu, X. Sun, H. Peng, *J. Mater. Chem. C* **2016**, *4*, 2127.
[30] M. Kolle, B. Zheng, N. Gibbons, J. J. Baumberg, U. Steiner, *Opt. Express* **2010**, *18*, 4356.
[31] M. C. Fuertes, S. Colodrero, G. Lozano, A. R. González-Elipe, D. Grosso, C. Boissière, C. Sánchez, G. J. A. A. Soler-Illia, H. Míguez, *J. Phys. Chem. C* **2008**, *112*, 3157.

[32] S. Y. Choi, M. Mamak, G. von Freymann, N. Chopra, G. A. Ozin, *Nano Lett.* **2006**, *6*, 2456.
[33] P. Lova, G. Manfredi, L. Boarino, A. Comite, M. Laus, M. Patrini, F. Marabelli, C. Soci, D. Comoretto, *ACS Photon.* **2015**, *2*, 537.
[34] R. A. Potyrailo, R. K. Bonam, J. G. Hartley, T. A. Starkey, P. Vukusic, M. Vasudev, T. Bunning, R. R. Naik, Z. Tang, M. A. Palacios, M. Larsen, L. A. Le Tarte, J. C. Grande, S. Zhong, T. Deng, *Nat. Commun.* **2015**, *6*, 7959.
[35] R. A. Potyrailo, H. Ghiradella, A. Vertiatchikh, K. Dovidenko, J. R. Cournoyer, E. Olson, *Nat. Photon.* **2007**, *1*, 123.
[36] J. M. Weissman, H. B. Sunkara, A. S. Tse, S. A. Asher, *Science* **1996**, *274*, 959.
[37] S. Torino, L. Conte, M. Iodice, G. Coppola, R. D. Prien, *Sens. Biosens. Res.* **2017**, *16*, 74.
[38] G. Gauglitz, M. Reichert, *Sens. Actuators, B* **1992**, *6*, 83.
[39] G. Harsányi, *Sens. Rev.* **2000**, *20*, 98.
[40] C. Fenzl, T. Hirsch, O. S. Wolfbeis, *Sensors* **2012**, *12*, 16954.
[41] Z. Mao, J. Wang, Y. Gong, H. Yang, S. Zhang, *Micromachines* **2018**, *9*, 606.
[42] C. Elosua, I. R. Matias, C. Bariain, F. J. Arregui, *Sensors* **2006**, *6*, 1440.
[43] X. Li, C. Yang, S. Yang, G. Li, *Sensors* **2012**, *12*, 12519.
[44] A. C. Arsenault, T. J. Clark, G. von Freymann, L. Cademartiri, R. Sapienza, J. Bertolotti, E. Vekris, S. Wong, V. Kitaev, I. Manners, R. Z. Wang, S. John, D. Wiersma, G. A. Ozin, *Nat. Mater.* **2006**, *5*, 179.
[45] J. C. Thomas, J. E. Trend, N. A. Rakow, M. S. Wendland, R. J. Poirier, D. M. Paolucci, *Sensors* **2011**, *11*, 3267.
[46] L. Spinelle, M. Gerboles, G. Kok, S. Persijn, T. Sauerwald, *Sensors* **2017**, *17*, 1520.
[47] *Wearable Electronics and Photonics*, 1st ed. (Ed: X. Tao), Woodhead Publishing, Sawston, UK **2005**.
[48] G. M. Murch, *IEEE Comput. Graph. Appl.* **1984**, *4*, 48.
[49] G. Wald, *Science* **1964**, *145*, 1007.
[50] R. Serway, J. Faughn, C. Vuille*College Physics*, Cengage Learning, Boston, MA **2008**.
[51] *Fundamentals of Human-Computer Interaction* (Ed: A. Monk), Academic Press, London **1985**.
[52] K. Moutzouris, M. Papamichael, S. C. Betsis, I. Stavrakas, G. Hloupis, D. Triantis, *Appl. Phys. B* **2014**, *116*, 617.
[53] J. Rheims, J. Köser, T. Wriedt, *Meas. Sci. Technol.* **1997**, *8*, 601.
[54] S. Kedenburg, M. Vieweg, T. Gissibl, H. Giessen, *Opt. Mater. Express* **2012**, *2*, 1588.
[55] K. Kerl, H. Varchmin, *J. Mol. Struct.* **1995**, *349*, 257.
[56] *CRC Handbook of Chemistry and Physics: A Ready-Reference Book of Chemical and Physical Data*, 88th ed. (Ed: D. R. Lide), CRC, Boca Raton, FL **2008**.